Fitting-based Cutting Force Estimation for Machine Tool with Encoder Resolution Analysis

Takumi Hayashi, Hiroshi Fujimoto
The University of Tokyo
5-1-5, Kashiwanoha, Kashiwa, Chiba, 277-8561, Japan
hayashi.takumi18@ae.k.u-tokyo.ac.jp, fujimoto@k.u-tokyo.ac.jp

Yoshihiro Isaoka, Yuki Terada
DMG MORI CO., LTD.
2-1, Sanjohonmachi, Nara, Nara, 630-8122, Japan
yo-isaoka@dmgmori.co.jp, yk-terada@dmgmori.co.jp

***Abstract*—The cutting process with machine tools plays an important role in the industry. Cutting force is a crucial factor in monitoring the tool status, and thus its sensorless estimation is gaining attention. The aim of this study is to develop a practical cutting force estimation. In this study, the encoder resolution is focused on, and the effect of encoder resolution on cutting force estimation is analyzed. Then, a cutting force estimation method robust to the quantization of the encoder signal is proposed. The experiments with an actual machine tool are performed, and the effectiveness of the proposed approach is demonstrated.**

***Index Terms*—Machine tool, cutting force estimation, two-inertia system, disturbance observer.**

I. Introduction

Automatic machining with machine tools is widely employed in the industry. Especially the cutting process plays an important role. Because the accuracy of the cutting process strongly influences product quality, the accuracy of the cutting process is of great importance.

Tool wear and tool breakage are well-known causes of machining errors. Therefore, a detection method for tool wear and breakage is required. The cutting force, generated by contacts between the tool and the workpiece, reflects the tool condition [1], and thus it is a good index for tool condition monitoring. A dynamometer can measure the cutting force directly; however, some issues, e.g., high cost, sensor placement, wiring, and measurement calibration, prevent its industrial application, and its uses are limited to research. Therefore, additional sensorless estimation methods of cutting force have been studied actively.

Recently, linear scales (load-side encoders) that can directly measure the stage position of machine tools (load-side position) have become popular for improving servo performance. Accordingly, various effective utilization of the load-side position has been studied, e.g. [2]. Sensorless cutting force estimation methods using the stage position acquired by the linear scale have been attracting attention [3], [4]. The method is based on disturbance observer (DOB) [5], [6], and an intuitive design is possible. Because of its simplicity, the DOB-based method is used in a wide range of areas of force estimation and control, e.g., [7], [8]. Our research group also proposed a sensorless cutting force estimation method robust to the mechanical parameter variation [9], [10].

However, few studies have verified cutting force estimation with machine tools used in the actual industry. The aim of this study is to analyze the cutting force estimation with an actual machine tool and develop a practical estimation method. Unlike machine tools for research objectives, the encoder (rotary encoder and linear scale) resolution of machine tools in the industry is still limited. First, the influence of the encoder resolution on cutting force estimation is analyzed in this study. The analysis reveals that the encoder resolution greatly influences cutting force estimation. Therefore, this study proposes a fitting-based cutting force estimation. The proposed approach is achieved by local curve-fitting of the encoder signals and the moving horizon approach. The proposed approach is validated through experiments with the actual machine tool.

Fig. 1. Experimental setup: CMX 1100V from DMG MORI CO., LTD.

The contributions of this study are as follows:

1) A cutting force estimation method is introduced and analyzed regarding the encoder resolution. It turns out that the quantization of the encoder signal has a large negative impact on cutting force estimation.
2) To address the above issue, a fitting-based cutting force estimation is proposed.
3) The proposed approach is validated through experiments with an industrial machine tool.

The remainder of this paper is organized as follows. The experimental setup is introduced in Section II. Then, Section III presents the conventional cutting force estimation. The method is analyzed regarding the encoder resolution in Section IV.

Next, a cutting force estimation method by curve-fitting is proposed in Section V. The proposed method is validated through experiments in Section VI. Finally, Section VII concludes this paper.

II. Experimental Setup

This section introduces the experimental setup.

A. System Configuration

The experimental setup, CMX 1100V from DMG MORI CO., LTD, is shown in Fig. 1. This setup is an industrial vertical machining center.

In the experimental setup, a ball-screw-driven stage is used as a feed system. The stage moves in two axes; x and y axis. A rotary encoder is attached to the motor on each axis, and a linear scale is attached to the stage. Full-closed control with the linear scale for stage position control is implemented. In this study, only the x axis motion is considered. Therefore, only the x axis data are treated in the remainder of this paper.

When the cutting process is carried out, a workpiece and dynamometer are fixed on the stage. The dynamometer (9255C from Kistler) is used only to validate the cutting force estimation. Furthermore, the tool is rotated by the spindle motor to cut the workpiece.

B. Modeling

Because the ball-screw connects the motor and the stage, the ball-screw-driven stage is often modeled as a two-inertia system [11]. The block diagram of the system is illustrated in Fig. 2.

The motor-side and stage-side equations of motion are given by

$$J_{\mathrm{m}}\dot{\omega}_{\mathrm{m}} = T_{\mathrm{m}} - D_{\mathrm{m}}\omega_{\mathrm{m}} - T_{\mathrm{nf}} - RF_{\mathrm{a}}, \tag{1}$$

$$M_{\mathrm{t}}\dot{v}_{\mathrm{t}} = F_{\mathrm{a}} - C_{\mathrm{t}}v_{\mathrm{t}} - F_{\mathrm{nf}} - F_{\mathrm{cut}}, \tag{2}$$

where $\omega_{\mathrm{m}} = \dot{\theta}_{\mathrm{m}}$ and $v_{\mathrm{t}} = \dot{x}_{\mathrm{t}}$ denote the motor angular velocity and stage velocity, respectively. The axial force of ball-screw denoted as F_{a} is derived by

$$F_{\mathrm{a}} = K(R\theta_{\mathrm{m}} - x_{\mathrm{t}}). \tag{3}$$

Here, the symbols in (1), (2), and (3) are as follows. J_{m} is a motor inertia, and D_{m} is a motor-side viscosity coefficient. K is a ball-screw stiffness, and R is a ball-screw rotation-to-translation ratio. M_{t} is a stage mass, and C_{t} is a stage-side viscosity coefficient. T_{m} is a motor torque, and T_{nf} is a motor-side nonlinear friction. F_{cut} is a cutting force, and F_{nf} is a stage-side nonlinear friction.

From (1), (2), and (3), the transfer function from motor torque T_{m} to motor angle θ_{m} is derived as (4).

A stepped-sine torque is applied to the motor for system identification, and the motor angle is measured. The result of system identification is shown in Fig. 3. Based on the frequency response data shown in Fig. 3 and the model (4), the mechanical parameters are identified. The identification results are summarized in Table I. Note that there is a mismatch between the frequency response data and its model around the resonance frequency (around $100\,\mathrm{Hz}$). This is because the motor-side and stage-side viscosity coefficients are identified by the constant velocity drive experiments of the stage.

TABLE I
Parameters of experimental setup.

Symbol	Description	Value
J_{m}	motor inertia	$4.06 \times 10^{-3}\,\mathrm{kgm^2}$
D_{m}	motor-side viscosity coefficient	$7.61 \times 10^{-3}\,\mathrm{Nms/rad}$
K	ball-screw stiffness	$1.03 \times 10^{8}\,\mathrm{N/m}$
R	ball-screw rotation-to-translation ratio	$1.91 \times 10^{-3}\,\mathrm{m/rad}$
M_{t}	stage mass	$2.60 \times 10^{2}\,\mathrm{kg}$
C_{t}	stage-side viscosity coefficient	$1.53 \times 10^{3}\,\mathrm{Ns/m}$

III. Cutting Force Estimation

In this section, the DOB-based cutting force estimation method is presented. First, the axial force is estimated based on the motor-side DOB. Then, the stage-side DOB estimates the cutting force. The block diagram is depicted in Fig. 4 [12].

From Fig. 2, the axial force estimate $\hat{F}_{\mathrm{a}}$ is given from the motor-side DOB by

$$Q\hat{F}_{\mathrm{a}} = \frac{1}{R}\big\{Q(T_{\mathrm{m}} - T_{\mathrm{nf}}) - Q\big(J_{\mathrm{m}}s^2 + D_{\mathrm{m}}s\big)\theta_{\mathrm{m}}\big\}. \tag{5}$$

Here, Q is a second-order low-pass filter (LPF) which makes $Q\big(J_{\mathrm{m}}s^2 + D_{\mathrm{m}}s\big)$ proper.

Then, the cutting force estimate $\hat{F}_{\mathrm{cut}}$ is derived from the stage-side DOB as

$$\hat{F}_{\mathrm{cut}} = Q\Big(\hat{F}_{\mathrm{a}} - F_{\mathrm{nf}}\Big) - Q\big(M_{\mathrm{t}}s^2 + C_{\mathrm{t}}s\big)x_{\mathrm{t}}. \tag{6}$$

From (5) and (6), the cutting force estimate $\hat{F}_{\mathrm{cut}}$ is given by

$$\begin{aligned}\hat{F}_{\mathrm{cut}} = \frac{Q}{R}T_{\mathrm{m}} - \frac{Q}{R}\big(J_{\mathrm{m}}s^2 + D_{\mathrm{m}}s\big)\theta_{\mathrm{m}} \\ - Q\big(M_{\mathrm{t}}s^2 + C_{\mathrm{t}}s\big)x_{\mathrm{t}} - Q\left(\frac{T_{\mathrm{nf}}}{R} + F_{\mathrm{nf}}\right)\end{aligned} \tag{7}$$

In this section, the DOB-based cutting force estimation method is introduced based on the block diagram and the transfer function. The method can also be derived from the state-space representation and the state observer; see [9].

IV. Encoder Resolution Analysis for Cutting Force Estimation

In this section, the effect of the quantization error on cutting force estimation is analyzed based on the discrete Lyapunov equation [13].

When the encoder's resolution is denoted as q, the quantization error of the encode signal, ξ, has a uniform distribution whose probability density function $f(\xi)$ is given by

$$f(\xi) = \begin{cases} \dfrac{1}{q} & \left(-\dfrac{q}{2} \le \xi \le \dfrac{q}{2}\right) \\ 0 & (\text{otherwise}) \end{cases}. \tag{8}$$

$$G_{\theta_{\rm m}T_{\rm m}} = \frac{\theta_{\rm m}}{T_{\rm m}} = \frac{M_{\rm t}s^2 + C_{\rm t}s + K}{J_{\rm m}M_{\rm t}s^4 + (J_{\rm m}C_{\rm t} + M_{\rm t}D_{\rm m})s^3 + \{K(J_{\rm m} + R^2M_{\rm t}) + D_{\rm m}C_{\rm t}\}s^2 + K(D_{\rm m} + R^2C_{\rm t})s}. \tag{4}$$

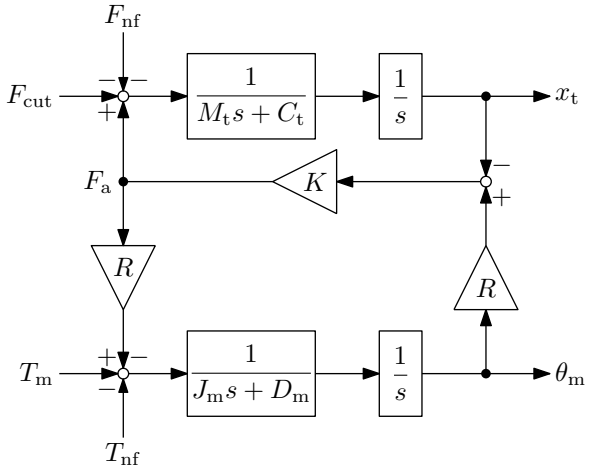

Fig. 2. Block diagram of a two-inertia system.

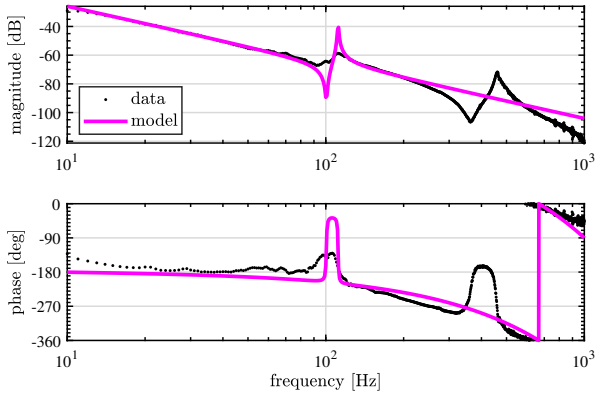

Fig. 3. Frequency response data from motor torque to motor angle of experimental setup. The model includes the time delay.

The average value and variance of the quantization error are given by

$$E\{\xi\} = 0, \tag{9}$$

$$E\{\xi^2\} = \int_{-q/2}^{q/2} \frac{1}{q}\xi^2 \, {\rm d}\xi = \frac{q^2}{12}, \tag{10}$$

where $E\{\bullet\}$ denotes the average value of $\bullet$. Furthermore, the cross-correlation function of the quantization error is given by

$$E\{\xi(t_1)\xi(t_2)\} = 0 \quad (t_1 \neq t_2). \tag{11}$$

Here, a linear discrete-time single-input single-output system G is considered, which is driven by the quantization error and given by

$$x[k+1] = Ax[k] + b\xi[k],\ y[k] = cx[k] + d\xi[k]. \tag{12}$$

According to (9)–(12), the output variance is derived as

$$E\{y^2[k]\} = cE\{x[k]x^\top[k]\}c^\top + d^2E\{\xi^2[k]\}. \tag{13}$$

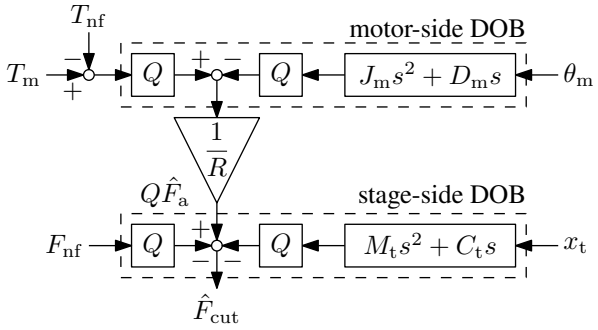

Fig. 4. Block diagram of cutting force estimation.

From (12), the following equations hold in the steady-state:

$$X = AXA^\top + E\{\xi^2\}bb^\top, \quad X = E\{xx^\top\}. \tag{14}$$

Thus, the output variance due to the quantization error is calculated as (13) from the solution of (14).

Based on (7) and (13), the effect of the quantization error on cutting force estimation is analyzed. Fig. 5 shows the cutting force estimation variance as functions of the resolutions of the rotary encoder and linear scale. The cutoff frequencies of the LPF Q used in the estimation is $150\,{\rm Hz}$, $300\,{\rm Hz}$, and $450\,{\rm Hz}$. Moreover, the dashed lines denote the resolutions of the encoders of the experimental setup shown in Fig. 1. The sampling frequency of the estimation is $1\,{\rm ms}$.

Fig. 5 indicates that the current encoder resolutions of this experimental setup cause the large estimation variance. Furthermore, the estimation variance becomes more significant when the cutoff frequency of the LPF Q is increased for high bandwidth cutting force estimation. From the above discussion, it is difficult to directly apply the approach (7) to cutting force estimation due to the current encoder resolution. In the next section, the solution to this problem is presented.

V. Proposed Fitting-based Cutting Force Estimation

The problem in cutting force estimation is that the quantization error of the encoder signal is amplified by DOB. In this study, therefore, the effect of the quantization error is reduced by estimating the true value from the quantized signal. This is achieved by local curve-fitting of the quantized signal and the moving horizon approach. Then, the cutting force is estimated with the fitted encoder signals. The block diagram of the proposed cutting force estimation is presented in Fig. 6.

A. Local Curve-fitting and Selection of Basis Function

First, the encoder signals are curve-fitted to estimate the true values. Basis functions for fitting $2N+1$ quantized local data $\{y_{\rm q}[i]\}_{i=k-N,\ldots,k,\ldots,k+N}$ is considered. Here,

$$y_{\rm q}[i] = y[i] + \xi[i], \quad y \in \{\theta_{\rm m},\, x_{\rm t}\} \tag{15}$$

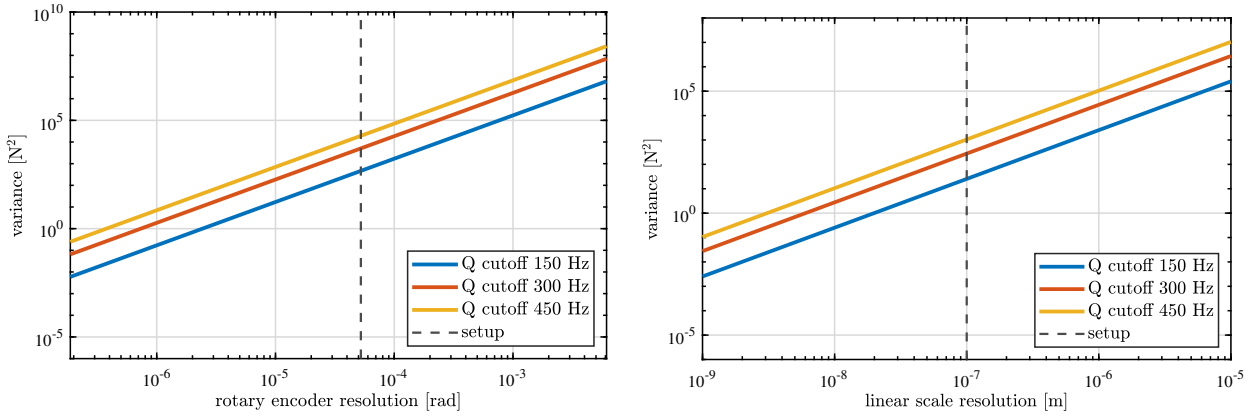

(a) Rotary encoder.

(b) Linear scale.

Fig. 5. Effect of quantization error on cutting force estimation.

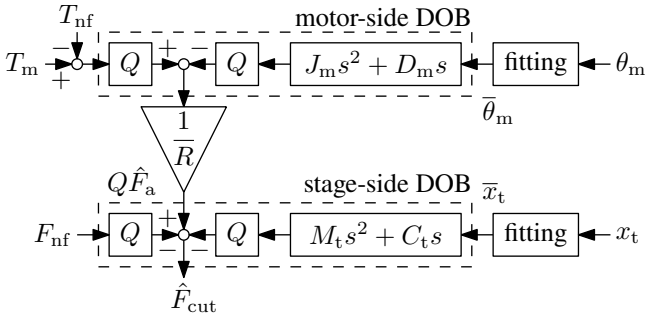

Fig. 6. Block diagram of the proposed cutting force estimation.

holds where y_q is a quantized signal, and y is a true signal. In addition, i denotes the time index, and k denotes the current time index with the sampling period T_s. The quantized local data are fitted with the basis functions and parameters as follows:

$$f(t) = \boldsymbol{\psi}(t)\boldsymbol{\theta}, \tag{16}$$

where $f(t)$, $\boldsymbol{\psi}$, and $\boldsymbol{\theta}$ are the fitted curve, basis functions, and parameters, respectively.

The selection of the basis functions is a key issue. While a polynomial is sometimes used for curve-fitting of quantized data [14], this study employs other basis functions. The cutting force mainly consists of frequency components integer multiples of the spindle rotation speed, and the encoder signals are affected by the cutting force. Furthermore, the cutting process is done when the stage moves at a constant velocity in this study. Therefore, the basis functions and parameters are selected as follows in this study:

$$f(t) = a_0 + a_1 t + \sum_{i=1}^{N_\mathrm{max}} \left(a_{\mathrm{s}i}\sin(i\omega_\mathrm{s}t) + a_{\mathrm{c}i}\cos(i\omega_\mathrm{s}t)\right), \tag{17}$$

$$\boldsymbol{\psi}(t) = \begin{bmatrix} 1 & t & \sin(\omega_\mathrm{s}t) & \cdots & \cos(N_\mathrm{max}\omega_\mathrm{s}t) \end{bmatrix}, \tag{18}$$

$$\boldsymbol{\theta} = \begin{bmatrix} a_0 & a_1 & a_{\mathrm{s}1} & \cdots & a_{\mathrm{c}N_\mathrm{max}} \end{bmatrix}^\top, \tag{19}$$

with the spindle rotation speed ω_s and the maximum order of curve-fitting N_max. Based on the above discussion, the local curve-fitting problem is formulated as follows:

$$\boldsymbol{\theta}_k = \arg\min ||\boldsymbol{\beta}_k - \boldsymbol{\Psi}_k\theta||_2^2, \tag{20}$$

$$\boldsymbol{\beta}_k = \begin{bmatrix} y_q[k-N] & \cdots & y_q[k] & \cdots & y_q[k+N] \end{bmatrix}^\top, \tag{21}$$

$$\boldsymbol{\Psi}_k = \begin{bmatrix} \boldsymbol{\psi}[k-N] & \cdots & \boldsymbol{\psi}[k] & \cdots & \boldsymbol{\psi}[k+N] \end{bmatrix}^\top. \tag{22}$$

Here, $2N_\mathrm{max} + 2 < 2N + 1$ is assumed.

The optimization problem (20) is solved by the least-square method and has a unique solution

$$\boldsymbol{\theta}_k = \left(\boldsymbol{\Psi}_k^\top\boldsymbol{\Psi}_k\right)^{-1}\boldsymbol{\Psi}_k^\top\boldsymbol{\beta}_k \tag{23}$$

when $\left(\boldsymbol{\Psi}_k^\top\boldsymbol{\Psi}_k\right)^{-1}$ exists.

B. Moving Horizon Approach

Once (20) is solved, the fitted curve is calculated as

$$f_k(t) = \boldsymbol{\psi}(t)\boldsymbol{\theta}_k. \tag{24}$$

Therefore, the estimated true value $\overline{y}[k]$ is given by

$$\overline{y}[k] = f_k(kT_\mathrm{s}). \tag{25}$$

Next, the time index is updated from k to $k+1$. Then, the same operation is repeated. In other words, $\boldsymbol{\theta}_{k+1}$ is solved as (20) with the one-sample updated quantized local data $\{y_\mathrm{q}[i]\}_{i=k-N+1,\ldots,k+1,\ldots,k+N+1}$. The estimated value is calculated as (20).

This moving horizon approach is illustrated in Fig. 7.

C. Cutting Force Estimation with Fitted Data

The cutting force is estimated with the estimated true values $\overline{\theta}_\mathrm{m}$ and $\overline{x}_\mathrm{t}$ as follows:

$$\hat{F}_\mathrm{cut} = \frac{Q}{R}T_\mathrm{m} - \frac{Q}{R}\left(J_\mathrm{m}s^2 + D_\mathrm{m}s\right)\overline{\theta}_\mathrm{m} - Q\left(M_\mathrm{t}s^2 + C_\mathrm{t}s\right)\overline{x}_\mathrm{t} - Q\left(\frac{T_\mathrm{nf}}{R} + F_\mathrm{nf}\right) \tag{26}$$

The block diagram is shown in Fig. 6.

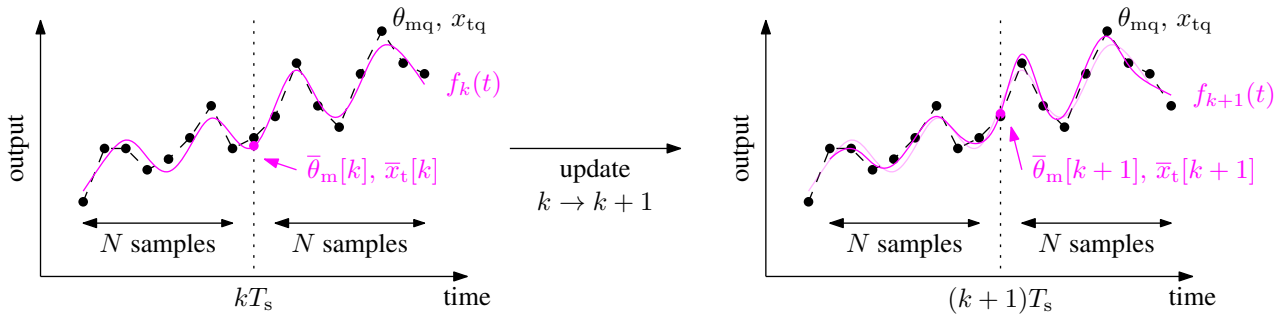

Fig. 7. Schematic of moving horizon approach for output fitting.

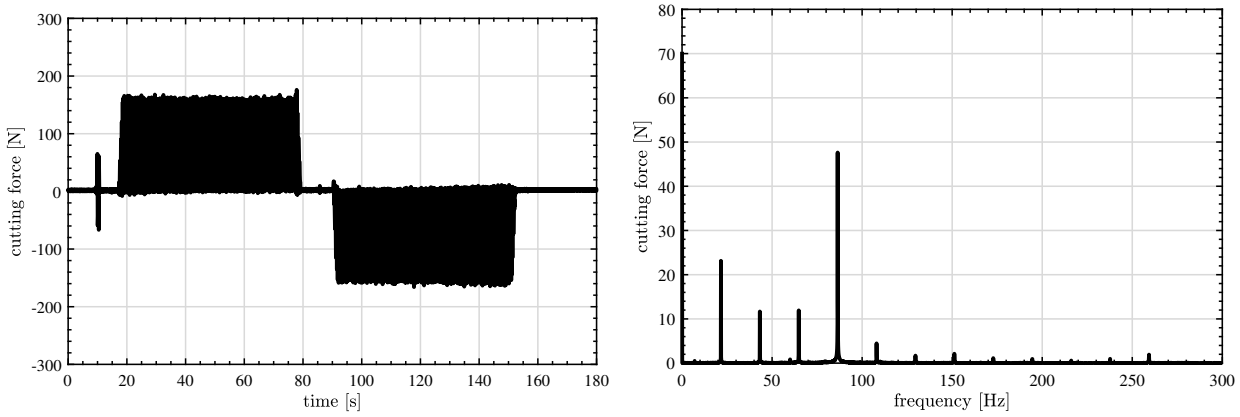

(a) Cutting force.

(b) Frequency domain analysis of cutting force

Fig. 8. Measured cutting force in experiment.

VI. Validation

In this section, the proposed approach presented in Section V is validated through the experiments with the setup shown in Fig. 1.

A. Experimental Condition

The experiment for cutting force estimation is described. First, the stage moves in the negative direction, and the cutting process is carried out when the stage velocity is constant. The stage velocity is set as $140\,\mathrm{mm/s}$, and the spindle rotation speed is set as $1300\,\mathrm{rpm}$ ($\omega_{\mathrm{s}} = 2\pi \cdot 21.7\,\mathrm{rad/s}$). Then, the stage stops. Next, the stage moves in the positive direction, and the cutting process is done similarly when the stage velocity is constant. Finally, the stage stops, and the experiment finishes.

The measured cutting force is illustrated in Fig. 8. Fig. 8(a) shows the time-domain data. The result of frequency-domain analysis of a part of time-domain data is shown in Fig. 8(b). It is observed that the cutting force has large components at integer multiples of the spindle rotation speed.

B. Estimation Result

Fig. 9 shows the cutting force estimation result. The legend "conv." denotes the cutting force estimation (7) without curve-fitting, while the legend "prop." denotes the cutting force estimation (26) with curve-fitting. Here, the LPF Q used in the cutting force estimation is a second-order filter whose cutoff frequency is $150\,\mathrm{Hz}$. Furthermore, $N_{\max}$ used in the proposed approach is 4 because the number of blades of the tool used in the experiment is four. N is set as 10.

From Fig. 9(a) and Fig. 9(c), it is clear that the estimation noise is reduced by signal curve-fitting. In the frequency domain shown in Fig. 9(b) and Fig. 9(d), the estimation noise in the high-frequency range decreases. As a result, the estimation result becomes close to the measurement result by introducing curve-fitting. Therefore, the effectiveness of the proposed approach is verified. Note that the comparison between the measured and estimated instantaneous values shown in Fig. 8 and Fig. 9 does not make sense because the measurement of cutting force by the dynamometer and the measurement of servo data (e.g., motor torque) by the servo amplifier is not synchronized.

VII. Conclusion

In this study, a fitting-based cutting force estimation is proposed to address the issue caused by the quantization of the encoder signals. In the proposed approach, the true values of the encoder signals are estimated from the quantized signals by curve-fitting. The experiment is performed, and the effectiveness of the proposed approach is demonstrated.

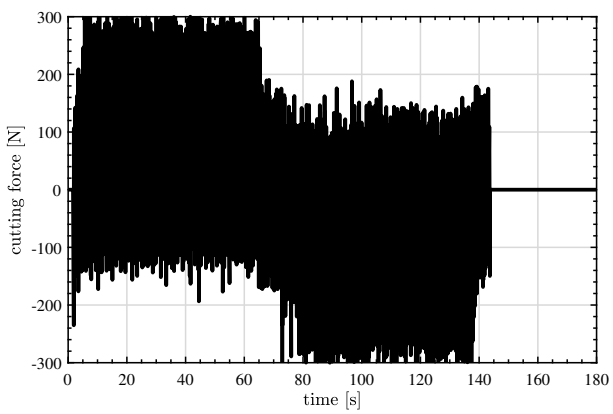

(a) Conventional method without curve-fitting.

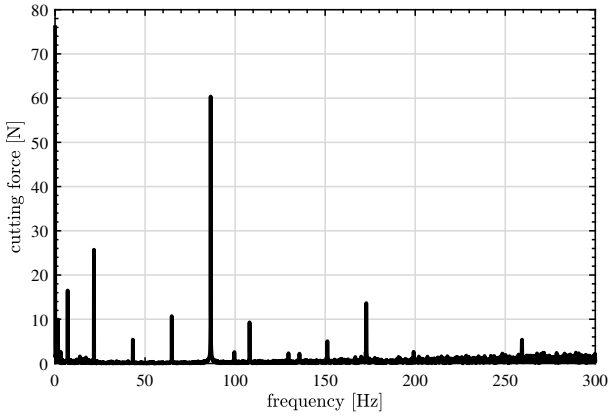

(b) Frequency domain analysis of conventional method without curve-fitting.

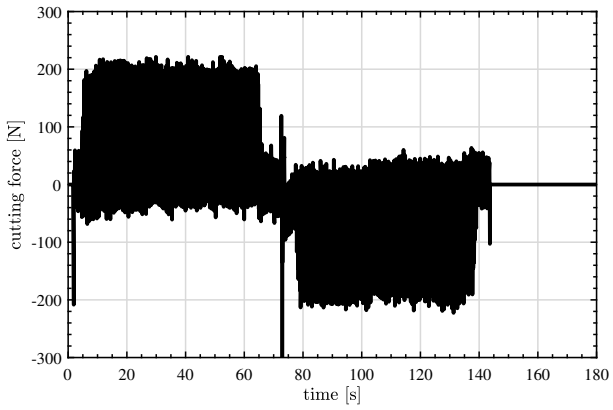

(c) Proposed method with curve-fitting.

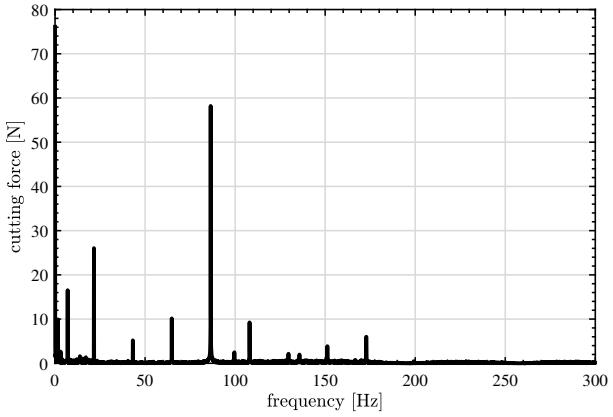

(d) Frequency domain analysis of proposed method with curve-fitting.

Fig. 9. Estimated cutting force in experiment.

REFERENCES

[1] N. Li, Y. Chen, D. Kong, and S. Tan, "Force-based tool condition monitoring for turning process using v-support vector regression," *Int. J. Adv. Manuf. Technol.*, vol. 91, no. 1-4, pp. 351–361, 2017.

[2] S. Yamada and H. Fujimoto, "Precise Joint Torque Control Method for Two-inertia System with Backlash Using Load-side Encoder," *IEEJ J. Ind. Appl.*, vol. 8, no. 1, pp. 75–83, 2019.

[3] Y. Yamada and Y. Kakinuma, "Sensorless cutting force estimation for full-closed controlled ball-screw-driven stage," *Int. J. Adv. Manuf. Technol.*, vol. 87, no. 9-12, pp. 3337–3348, 2016.

[4] Y. Yamada, S. Yamato, and Y. Kakinuma, "Mode decoupled and sensorless cutting force monitoring based on multi-encoder," *Int. J. Adv. Manuf. Technol.*, vol. 92, no. 9-12, pp. 4081–4093, 2017.

[5] W.-H. Chen, J. Yang, L. Guo, and S. Li, "Disturbance-Observer-Based Control and Related Methods—An Overview," *IEEE Trans. Ind. Electron.*, vol. 63, no. 2, pp. 1083–1095, 2016.

[6] E. Sariyildiz, R. Oboe, and K. Ohnishi, "Disturbance Observer-Based Robust Control and Its Applications: 35th Anniversary Overview," *IEEE Trans. Ind. Electron.*, vol. 67, no. 3, pp. 2042–2053, 2020.

[9] S. Yamada and H. Fujimoto, "Minimum-Variance Load-Side External Torque Estimation Robust Against Modeling and Measurement Errors," *IEEJ J. Ind. Appl.*, vol. 9, no. 2, pp. 117–124, 2020.

[7] H. Kurumatani and S. Katsura, "Design of Nominal Parameters for Robust Sensorless Force Control Based on Disturbance Observer," *IEEJ J. Ind. Appl.*, vol. 8, no. 2, pp. 342–351, 2019.

[8] T. T. Phuong, K. Ohishi, and Y. Yokokura, "High-Performance Sensorless Force Control Using Superior Wideband and Periodicity-Cancellation Force Observer," *IEEJ J. Ind. Appl.*, p. 22000390, 2023.

[10] K. Ohno, H. Fujimoto, Y. Isaoka, and Y. Terada, "Adaptive Cutting Force Observer for Machine Tool Considering Stage Parameter Variation," in *2021 IEEE Int. Conf. Mechatronics*. IEEE, 2021.

[11] Y. Yoshiura, Y. Asai, and Y. Kaku, "Anti-resonance Vibration Suppression Control in Full-closed Control System," *IEEJ J. Ind. Appl.*, vol. 9, no. 3, pp. 311–317, 2020.

[12] M. Matsuoka, T. Murakami, and K. Ohnishi, "Vibration suppression and disturbance rejection control of a flexible link arm," in *Proc. IECON '95 - 21st Annu. Conf. IEEE Ind. Electron.*, vol. 2. IEEE, 1995, pp. 1260–1265.

[13] T. Emmei, S. Wakui, and H. Fujimoto, "Acceleration Noise Suppression for Geared In-Wheel-Motor Vehicles Using Double Encoder," *IEEE J. Emerg. Sel. Top. Ind. Electron.*, vol. 2, no. 1, pp. 53–60, 2021.

[14] H. Zhu, T. Sugie, and H. Fujimoto, "Smooth Output Reconstruction for Linear Systems with Quantized Measurements," *Asian J. Control*, vol. 17, no. 3, pp. 1039–1049, 2015.